ADVANCED MATERIALS

rials with optical chemical sensors allows the optical temperature compensation of optode signals. These so-called hybrid optodes have a temperature element integrated into the chemical sensing layer. Finally, there is a broad potential of the films for use as temperature-sensitive paint.

Experimental

Materials: Ruthenium(II)-tris-1,10-phenanthroline chloride hydrate (M_w: 712 g/mol, Aldrich, prod. no. 34,371-4); tetramethoxysilane (TMOS, Fluka, prod. no. 87 682); poly(acrylonitrile) (Faserwerk Kehlheim, technical grade); silicon rubber (Wacker, E4).

Preparation of Sol-Gel Sensor Membranes: 4.94 mL (33.3 mmol) tetramethoxysilane (2 g sol-gel matrix) was added to a solution of different amounts of (see Table 1) Ru(phen)$_3$Cl in 4 mL methanol and 2 mL distilled water. The sol-gel process was started by adding 0.4 mL of 0.1 N HCl. After a 10 min condensation reaction the solvents were removed within a few seconds at 30 torr and 100 °C. The dense sol-gel obtained was powdered and heated to 300 °C for 10 h. The cold powder was dispersed in 10 mL of methanol and a new sol-gel process was started by adding 2.47 mL of TMOS, 1 mL of distilled water, and 0.2 mL of 0.1 N HCl. While stirring, the solution was heated to 100 °C until dryness (~10 min) and then tempered at 300 °C for 2 h. Equal quantities of powder and silicone prepolymer E4 were mixed and spread onto the polyester support at a layer thickness of 250 μm. After 1 day of curing in ambient air the sensing layer was ready for use.

Preparation of PAN Sensor Membranes: Ru(phen)$_3$(PF$_6$)$_2$ (M_w: 985 g/mol) was precipitated from an aqueous Ru(phen)$_3$Cl$_2$ solution by adding NaPF$_6$ dissolved in water. Different amounts (see Table 1) of Ru(phen)$_3$(PF$_6$)$_2$ were added to a solution of 1.0 g of poly(acrylonitrile) in 10 mL of DMF. The cocktail was spread onto a 125 μm thick polyester support (Mylar, DuPont) in a wet layer thickness of 120 μm under nitrogen. After drying at room temperature under nitrogen, the membrane was tempered at 100 °C for 4 h. The resulting sensing layer was ready for use. From the volume employed, the dried layers are estimated to be 10 μm thick.

Experimental Set-Up: The excitation light of a blue LED (λ_{max} 470 nm, NSPB 500, Nichia) passing a blue glass filter (BG 12, Schott, Mainz) was sinusoidally modulated at 75 kHz using a two-phase lock-in amplifier (DSP830, Stanford Research Inc.). Luminescence was detected with a photomultiplier tube (H5701-02, Hamamatsu) equipped with a longpass filter (OG 570, Schott, Mainz). A bifurcated fiber bundle (n.a. 0.46, d = 2 mm, Laaber LWL GmbH) was used to separate the luminescence signal with a peak at 610 nm from backscattered blue excitation light.

Calibration and investigation of response time and reversibility were performed by immersing the sensors alternately in different water baths whose temperatures were controlled by a Lauda cryostat (RC6).

[1] K. T. V. Grattan, "Temperature Sensors", in *Fiber Optic Chemical Sensors and Biosensors* (Ed: O. S. Wolfbeis), CRC Press, Boca Raton, FL **1991**, Vol. 2, Ch. 15.

[2] *Optical Fiber Sensors: Principles and Components* (Eds: J. Dakin, B. Culshaw), Artech House, Boston, MA **1988**, Vol. 1.

[3] V. Bhatia, K. Murphy, R. May, R. Claus, T. Richard, T. Tran, J. Greene, J. Coate, *High Temp. Mater. Sci.* **1996**, *35*, 31.

[4] T. Pustelny, *Sens. Actuators A* **1995**, *A49*, 57.

[5] S. Gupta, T. Mizunami, T. Yamao, T. Shimomura, *Appl. Opt.* **1996**, *35*, 5202.

[6] K. A. Wickersheim, *Proc. SPIE—Int. Soc. Opt. Eng.* **1991**, *1584*, 3.

[7] J. S. McCormack, *Electron. Lett.* **1981**, *17*, 630.

[8] Z. Zhang, J. H. Herringer, N. Djeu, *Rev. Sci. Instrum.* **1997**, *68*, 2068.

[9] Y. L. Hu, Z. Y. Zhang, K. T. V. Grattan, A. W. Palmer, B. T. Meggitt, *Sens. Actuators A* **1997**, *63*, 85.

[10] G. Holst, R. Glud, M. Kühl, I. Klimant, *Sens. Actuators B* **1997**, *38–39*, 122.

[11] I. Klimant, O. S. Wolfbeis, *Anal. Chem.* **1995**, *67*, 3160.

[12] O. S. Wolfbeis, I. Klimant, T. Werner, C. Huber, U. Kosch, C. Krause, G. Neurauter, A. Dürkop, *Sens. Actuators B* **1998**, *51*, 17.

[13] J. N. Demas, B. A. DeGraff, *Anal. Chem.* **1991**, *63*, 829A.

[14] J. N. Demas, B. A. DeGraff, *Proc. SPIE—Int. Soc. Opt. Eng.* **1992**, *1796*, 71.

[15] G. Holst, O. Kohls, I. Klimant, B. König, M. Kühl, T. Richter, *Sens. Actuators B* **1998**, *51*, 163.

## Molecular Boxes Based on Hollow Organosilicon Micronetworks**

By *Olaf Emmerich*, *Norbert Hugenberg*, *Manfred Schmidt*,* *Sergei S. Sheiko*, *Frank Baumann*, *Bernward Deubzer*, *Johann Weis*, and *Jochen Ebenhoch*

Molecular boxes, or molecular containers, have become the subject of much investigation because of their potential applications as confined-reaction vessels, drug carriers, dye dispersants, etc. By far the majority of systems reported are based on micellar or vesicular structures,[1,2] which principally exhibit a more or less pronounced size and/or aggregation number fluctuation and which are often subject to shape changes. Form- and size-invariant containers were successfully prepared by polymerization of and in vesicles, mostly in the micrometer size range,[3–8] or by tedious multi-step branching reactions leading to dendrimers (dendritic boxes) of sub 10 nm size.[9–12] Also, colloidal templating has been successfully applied to produce hollow silicate spheres, 0.5–3 μm in size.[13–15] Surface-crosslinked hollow polymeric structures were prepared by crosslinking the shell of a block copolymer micelle and subsequent degradation of the core.[16] Based on our previous work, towards the preparation of homogeneous and core shell organosilicon micronetworks, [17–19] we report, in this paper, on the synthesis, characterization, and properties of hollow organosilicon micronetworks less than 50 nm in size. These exhibit a narrow size distribution and dissolve, as single particles, in common organic solvents such as toluene and tetrahydrofuran (THF).

Scheme 1 describes the synthetic route to the hollow micronetworks and is outlined, in detail, in the experimental section. In order to unambiguously distinguish hollow from solid structures, we compared the hollow micronetwork (sample HK70) with a homogeneously crosslinked sample (VK70) of identical crosslinking density (70:30 ratio of trifunctional to bifunctional monomers).

[*] Prof. M. Schmidt, O. Emmerich, N. Hugenberg
Institut für Physikalische Chemie
Johannes Gutenberg-Universität
D-55128 Mainz (Germany)

Dr. S. S. Sheiko
Organische und Makromolekulare Chemie, Universität Ulm
D-89069 Ulm (Germany)

Dr. F. Baumann, Dr. B. Deubzer, Dr. J. Weis, Dr. J. Ebenhoch
Wacker-Chemie GmbH
D-84480 Burghausen (Germany)
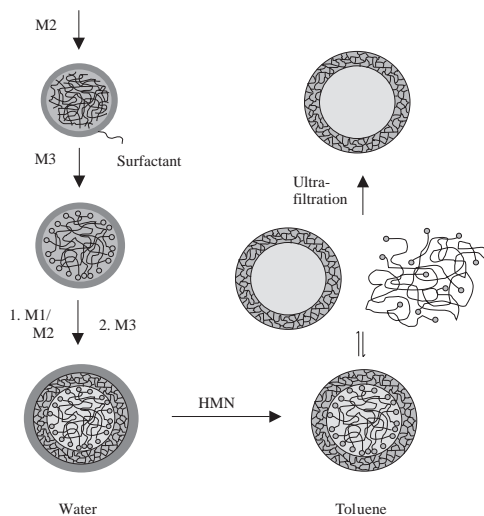
Scheme 1. Preparation of hollow organosilicon micronetworks. M2 = Me$_2$-Si(OMe)$_2$, M3 = Me$_3$SiOMe, M1 = MeSi(OMe)$_3$. (HMN is hexamethyldisilazane.)

Figure 1 shows the GPC (gel permeation chromatography) traces of both samples. The homogeneously cross-linked microspheres VK70 exhibited one narrow elution peak (Fig. 1a) whereas, for sample HK70, two elution peaks were detected (Fig. 1b). The first narrow peak originates from the hollow micronetworks whereas the second,
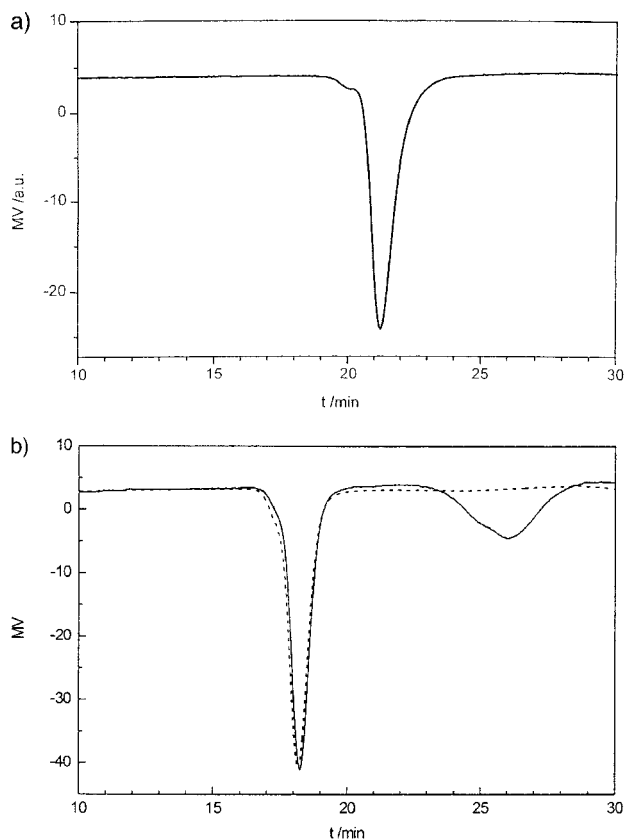

Fig. 1. GPC traces of a) homogeneous and b) hollow micronetworks. The dashed line shows the elugram of the hollow micronetworks after ultrafiltration.

broad peak, is caused by the fraction of linear poly(dimethylsiloxane) (PDMS) chains that have diffused out of the network core. As shown by the dashed line in Figure 1b, this linear fraction can be quantitatively removed by ultrafiltration. The molar mass of the linear PDMS was estimated to be in the range M_w = 2000–3000 g mol^{-1}.

The light scattering characterization of samples VK70 and HK70 confirmed the spherical and hollow structure, respectively, as listed in Table 1. The ratio, P, of the radius

Table 1. Light scattering characterization of the homogeneous (VK70) and hollow organosilicon micronetworks (HK70).

	HK70	VK70
R_g [nm]	26.7 ± 1	< 10
R_h [nm]	26.7	12.0
P	1.0	< 0.83
M_w [g mol^{-1}]	25.4×10^6	3.2×10^6
ρ [g cm^{-3}]	0.53 ± 0.05	0.73

of gyration, $R_g \equiv \langle S^2 \rangle_z^{1/2}$, to the hydrodynamic radius, $R_{DLS} \equiv \langle 1/R_h \rangle_z^{-1}$, was found to be $P = 1$ for HK70 and $P < 0.83$ for sample VK70 (Eq. 1).

$$P = R_g / R_{DLS} \qquad (1)$$

According to theory these are the expected values for hollow and full spheres, respectively. Likewise, the particle density (Eq. 2), derived from the molar mass and the hydrodynamic radius (N_A is the Avogadro constant), was about 30 % lower for HK70 ($\rho = 0.53$ g cm^{-3}) when compared to VK70 ($\rho = 0.73$ g cm^{-3}), but somewhat higher than that calculated from the outer radius $R_{DLS} = 26.7$ nm ($\rho = 0.45$ g cm^{-3}) and a shell thickness of $d = 6$ nm (see below).

$$\rho = \frac{3 M_w}{4 \pi N_A R_{DLS}^3} \qquad (2)$$

Since both the ratio P and the particle density may be significantly influenced even by the small polydispersity of the samples, X-ray scattering was utilized in order to investigate the inner structure of the micronetworks. The desmeared curves are shown in Figure 2a and Figure 2b for the homogeneous and hollow micronetworks, respectively.

The theoretical expression, for the particle scattering factor of a hollow sphere, is given in Equations 3 and 4[19] with $\upsilon = q \cdot R_a$ and $u = q \cdot R_i$, where q is the scattering vector, R_a and R_i are the outer and inner radii, respectively, and n_a, n_i, n_s are the refractive indices (for light scattering) or the electron densities (for X-ray scattering) of the shell, the core, and the solvent.

$$P(q) = \left(\frac{3}{1-\beta} \right)^2 \left(\frac{\sin\upsilon - \upsilon\cos\upsilon}{\upsilon^3} - \beta \frac{\sin u - u\cos u}{u^3} \right)^2 \qquad (3)$$

$$\beta = \frac{n_a - n_i}{n_a - n_s} \cdot \frac{R_i^3}{R_a^3} \qquad (4)$$

Since the particles exhibit a small, but significant polydispersity, the z-average particle scattering factor may be cal-
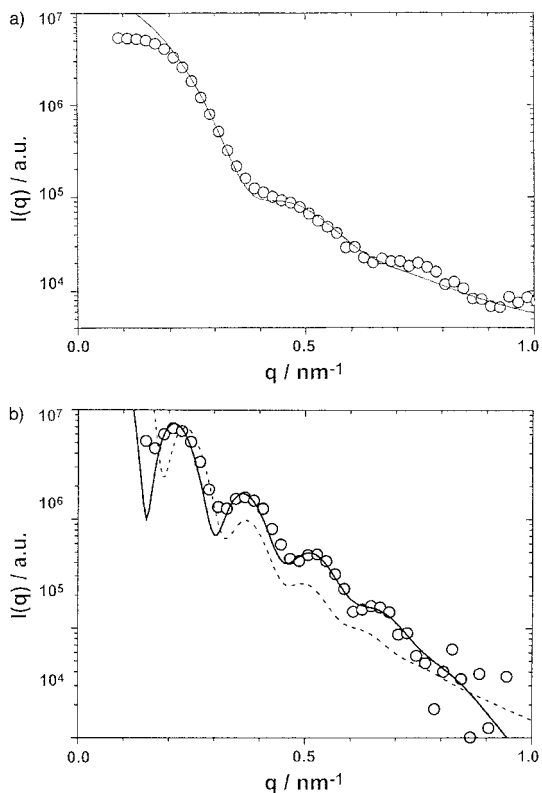
Fig. 2. X-ray scattering envelopes for a) the homogeneous and b) the hollow micronetworks. The solid curve in (a) represents Equation 9 with R_a = 11.0 nm and σ = 1.8 nm, whereas the solid line in (b) represents the hollow sphere according to Equation 6 with R_a = 23.0 nm, R_i = 17.5 nm, and σ = 1.85 nm. The dotted line for the homogeneous sphere, with R_a = 23.7 nm and σ = 1.85, systematically misses the minima and maxima of the experimental curve.

culated assuming a Gaussian distribution of the outer radius, R_a (Eq. 5), as described in Equation 6.

$$h(R_a) = \frac{1}{\sigma(2\pi)^{1/2}} \exp\left(\frac{-(R_a - \langle R_a \rangle)^2}{2\sigma^2}\right) \quad (5)$$

$$P_z(q) = \frac{\int_0^\infty h(R_a) \cdot R_a^6 \cdot (1-\beta)^2 \cdot P(q)\, dR_a}{\int_0^\infty h(R_a) R_a^6 (1-\beta)^2\, dR_a} \quad (6)$$

The inner radius was assumed to vary according to Equation 7 where f is a radius-independent constant that yields a mean shell thickness $\langle d \rangle$ as described in Equation 8.

$$R_i = f \cdot R_a \quad (7)$$

$$\langle d \rangle = \langle R_a \rangle - \langle R_i \rangle = \langle R_a \rangle \cdot (1-f) \quad (8)$$

In the limit $R_i = 0$, the combination of Equation 3 and Equation 6 reproduces the result for a homogeneous sphere (Eq. 9).

$$P_z(q) = \frac{\int_0^\infty h(R) R^6 \left[3(\sin(qR) - qR\cos(qR))/(qR)^3\right]^2 dR}{\int_0^\infty h(R) R^6\, dR} \quad (9)$$

For sample VK70 the best superposition of experiment and theory is achieved by using Equation 9, for a full sphere, which has an outer radius of R_a = 11.0 nm and σ = 1.8 nm (see Fig. 2a), which gives $\langle R_h^{-1} \rangle_z^{-1}$ = 12.3 nm, which is in almost perfect agreement with the light scattering result of R_{DLS} = 12.0 nm. For the hollow micronetwork, HK70, Equation 9 does not accurately represent the experimental data (dotted curve in Fig. 2b), whereas Equation 6, for a hollow sphere, provides a good description with R_a = 23.0 nm, R_i = 17.5 nm, σ = 1.85 nm (full curve in Fig. 2b), and the contrast $n_i = n_s$. From $R = \langle R_a \rangle_n$ = 23.0 nm and σ = 1.85 nm, the inverse z-average of the hydrodynamic radius $1/\langle R_h \rangle_z^{-1}$ was calculated to be 23.7 nm, which agrees well with the measured light scattering radius, R_{DLS} = 26.7 nm. Thus, the hollow nature of sample HK70 was confirmed by X-ray scattering. In addition, the mean thickness of the network shell was determined to be $\langle d \rangle$ = 5.5 nm. In order to obtain the thickness of the shell independently, by X-ray reflection and by scanning force microscopy (SFM), a monolayer of both hollow and full spheres was prepared by spin casting on a silicon wafer and on mica, respectively. The atomic force microscopy (AFM) image of the full and hollow spheres are shown in Figure 3a
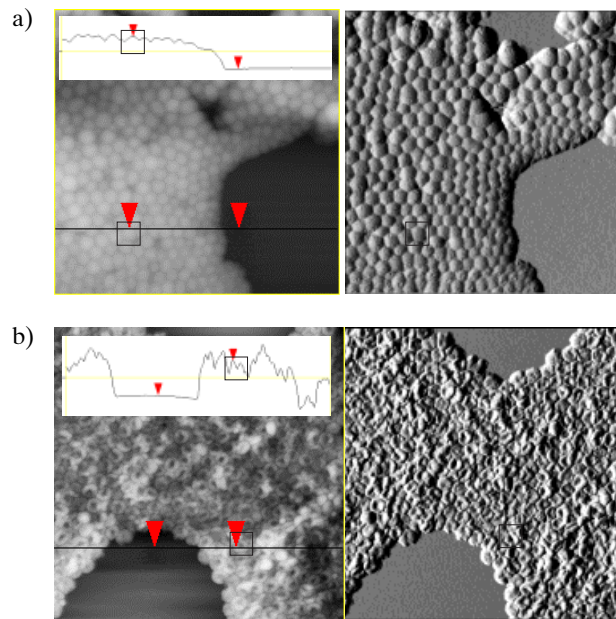

Fig. 3. SFM pictures in the height (left) and amplitude (right) mode of the a) homogeneous and b) hollow organosilicon micronetworks. The insets show the height profiles as discussed in the text.

and Figure 3b, respectively. The radius of the full spheres, R_{SFM} = 12 nm, coincides well with the scattering results. The height of the particles, h = 18 nm, however, is significantly less than twice the radius, R_{SFM}, which suggests that the dry spheres are somewhat deformed at the surface.

The hollow spheres, HK70 (Fig. 3b), are completely collapsed, resulting in pancake-like structures with a radius R_{SFM} = 25 nm and a height $h = 2d = 12 \pm 1$ nm. Again, the radius R_{SFM} coincides well with the dynamic light scatter-

ADVANCED MATERIALS

ing result and with the outer radius determined by X-ray scattering. The shell thickness, $d = 6.0 \pm 0.5$ nm, also confirms the X-ray scattering analysis yielding $d = 5.5$ nm as derived above. Moreover, a bulge of roughly 2–3 nm in height, at the rim of the collapsed micronetworks, becomes apparent from the topological plot (insert in Fig. 3b). Similar shapes are frequently observed for flat soccer balls.

The X-ray reflection curve, obtained from the collapsed monolayer of HK70, is shown in Figure 4, the fit of which
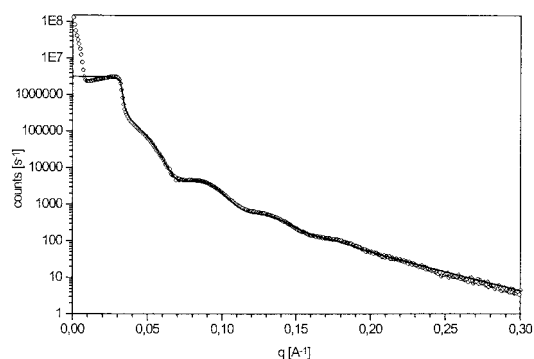

Fig. 4. X-ray reflection curve for a monolayer of hollow organosilicon micronetworks. The solid line represents the Fresnel fit with a layer thickness of $2d = 13.7$ nm.

yields a thickness of $2d = 13.7$ nm, i.e., a shell thickness of $d = 6.85$ nm thus confirming, qualitatively, the scattering and AFM results. This is somewhat surprising given the fact that a perfect continuous monolayer is not expected to form. However, the results from layers formed by spin casting solutions of different concentrations ($2 \, \text{g L}^{-1} \leq c \leq 5 \, \text{g L}^{-1}$) did not show any concentration dependence.

In order to establish to what extent the hollow micronetworks can be refilled with PDMS chains sample HK70 was dissolved in a solution of silicon oil (DMS-T11, $M = 5970 \, \text{g mol}^{-1}$, $\eta = 100$ cSt., Celest Inc.) in toluene (HK70/PDMS = 1:2 wt.-%). One drop of the solution was spin cast onto a freshly cleaved mica surface. After complete evaporation of the toluene the micronetworks were clearly swollen with PDMS, as impressively demonstrated in Figure 5. Whereas the lateral diameter is identical to the one of the collapsed micronetwork (i.e., $2R \simeq 50$ nm), the height is now significantly increased ($h = 33$ nm). Assuming a thickness of 6 nm for the network shell 56 vol.-% of the micronetwork core is filled with silicon oil. This demonstrates that the PDMS penetrates the micronetwork.

Besides the determination of the lateral and horizontal dimensions of the micronetwork, SFM provides a qualitative measure of the hardness of the investigated object. When operated in the tapping mode, the phase shift of the vibrating tip depends on the dissipation of energy caused by the interaction of the tip with the surface. The probed dimension may originate from the sample viscosity, friction between tip and sample, and adhesion.

Phase shifts are investigated for the present micronetworks utilizing a mixture of hard micronetworks, consisting
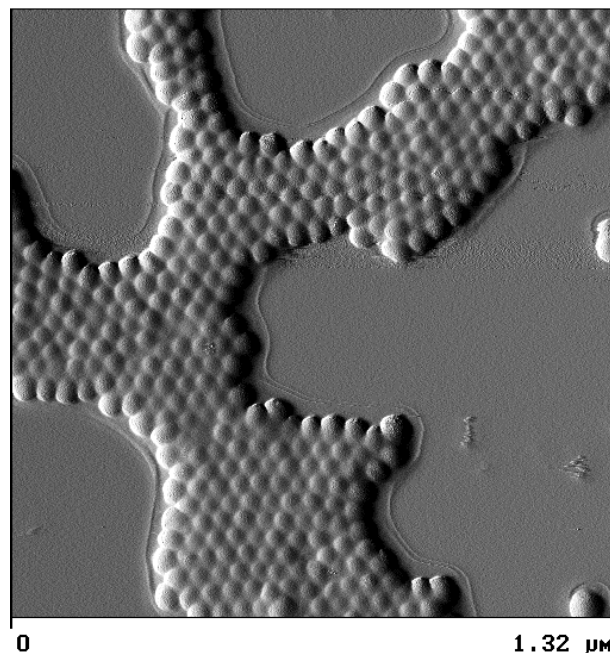

Fig. 5. Amplitude SFM picture of the hollow organosilicon micronetworks filled with linear PDMS chains.

of trifunctional monomers only, and of silicon oil filled, soft micronetworks, which were spin cast on mica. The phase contrast is shown in Figure 6, where an increasing phase shift, i.e., larger energy dissipation, is represented as a
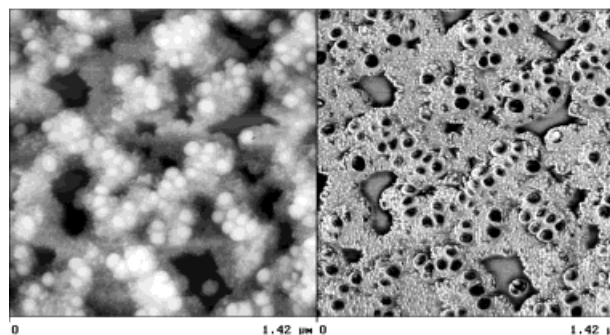

Fig. 6. SFM picture of a mixture of small and hard (fully crosslinked) organosilicon micronetworks and of large PDMS filled spheres (see Fig. 5). The phase contrast (right) is much more pronounced than the height mode (left), as discussed in the text.

darker gray tone. The smaller spheres ($R \approx 10$ nm) and the mica surface appear bright, which indicates small phase shifts, small elastic response, and large hardness, accordingly. The large black dots correspond to the particles filled with silicon oil, which clearly proves the soft elastic nature of the particles.

However, the present particles do not yet selectively accumulate substrates in their encapsulated inner volume. This could, principally, be achieved by decoration of the inner surface with hydrophilic groups, which would eventually allow a water pool to be placed inside a single micronetwork or by hydrophilization of the shell in order to

make the hydrophobic inner micronetwork water soluble. Experiments directed at the synthesis of hollow micronetworks, which exhibit two shells of different polarity, are currently in progress.

Experimental

The micronetworks were prepared, by the base catalyzed procedure, as described previously [17–19]. For the preparation of the hollow spheres (sample HK70) the surfactant benzethonium chloride (3.0 g, Aldrich, $M =$ 448 g mol^{-1}) was dissolved in water (125.0 g) containing NaOH (300 mg, 10 wt.-%). Dimethoxydimethylsilane (11.0 g) was added, with vigorous stirring, at room temperature over 1 h. After stirring for a further 12 h the silanol end groups of the PDMS chains were endcapped using methoxytrimethylsilane (100 mg).

A mixture of methytrimethoxysilane (10.0 g) and dimethoxydimethylsilane (4.0 g) was added over 1 h and the resultant mixture stirred for a further 5 h. In order to prevent the remaining reactive silanol groups from undergoing interparticle condensation, the endcapping procedure was repeated twice more, with methoxytrimethylsilane (2.5 g), before the removal of the surfactant. The dispersion was destabilized by the addition of methanol and centrifuged. The precipitate was washed three times with methanol, to remove the surfactant, and then dissolved in toluene.

At this stage the endcapping of the silanol groups is not yet quantitative. Therefore, hexamethyldisilazane (5.0 g, Wacker-Chemie GmbH, $M =$ 164 g mol^{-1}) was added to the toluene solution and the reaction mixture was stirred, at room temperature, for 12 h. The micronetworks were again precipitated with methanol, centrifuged and dried. A colorless, sticky residue was obtained.

In order to remove the linear PDMS chains from the core of the micronetworks the residue was dissolved in THF and ultrafiltered (Millipore cellulose 30 000) 4–5 times. The solvent was evaporated, the solid residue dissolved in benzene, and freeze-dried overnight. Yield: 3.5 g of a colorless powder. Sample VK70 was prepared as described previously [19].

Static and dynamic light scattering measurements were performed with standard equipment utilizing an ALV SP-86 goniometer, an ALV 3000 correlator, and a Spectra Physics 2060-11s Krypton ion laser light source (647.1 nm wavelength, 500 mW power) or an ALV SP-125 goniometer, an ALV 5000 correlator, and a Spectra Physics 2060-04s Argon ion laser light source (514.0 nm, 250 mW). Correlation functions were analyzed by the method of cumulants.

All samples described here exhibited normalized second cumulants of μ_2 < 0.05, and no angular dependence of the diffusion coefficients was observed. Before conducting any measurements the toluene solution (0.2 g L^{-1} < c < 1.5 g L^{-1}) was filtered through a 0.2 µm Millex FGN Teflon filter.

The refractive index increments were measured with a special, home-built, interferometer utilizing a small laser (Polytec, wavelength 543 nm or uniphase, 632 nm) [20].

Atomic force micrographs were recorded with a Nanoscope III instrument (Digital Instruments, St. Barbara, CA) operating in tapping mode at a resonance frequency of about 280 kHz. One drop of a 1 % solution of micronetworks in toluene was placed on a freshly cleaved mica surface and spin cast.

Ultrafiltration was performed in a 300 mL cell (Millipore XFUF 07601), equipped with a stirrer, utilizing membranes of regenerated cellulose (Millipore PLTK076 NMWL 30 000).

For X-ray reflection measurements (Siemens D500) one drop of the sample toluene solution (2 g L^{-1} < c < 5 g L^{-1}) was placed on a silica wafer and spin cast.

Small angle X-ray scattering (SAXS) experiments of the dissolved sample in THF (concentration 1 %–7 %) were performed with a Kratky camera (Paar, Austria) equipped with a capillar holder and a position-sensitive detector (Braun). Scattering profiles were desmeared using a standard procedure [21].

[1] H. Ringsdorf, B. Schlarb, J. Venzmer, *Angew. Chem.* **1988**, *100*, 117; *Angew. Chem. Int. Ed. Engl.* **1998**, *27*, 113.
[2] J. H. Fendler, *Adv. Polym. Sci.* **1994**, *113*, 1.
[3] J. Kurja, R. J. M. Nolte, I. A. Maxwell, A. L. German, *Polymer* **1993**, *34*, 2045.
[4] N. Poulin, E. Nakache, A. Pina, G. Levesque, *J. Polym. Sci.* **1996**, *34*, 729.
[5] S. L. Regen, J.-S. Shin, *J. Am. Chem. Soc.* **1984**, *106*, 5756.
[6] J. Murtagh, J. K. Thomas, *Faraday Discuss. Chem. Soc.* **1986**, *81*, 127.
[7] J. Hotz, W. Meier, *Langmuir* **1998**, *14*, 1031.
[8] J. Hotz, W. Meier, *Adv. Mater*. **1998**, *10*, 1387.
[9] G. R. Newkome, C. N. Moorefield, *Polym. Prepr. (Am. Chem. Soc., Div. Polym. Chem.)* **1993**, *34*, 75.
[10] C. J. Hawker, K. L. Wooley, J. M. J. Frechet, , *Polym. Prepr. (Am. Chem. Soc., Div. Polym. Chem.)* **1993**, *34*, 54.
[11] J. F. G. A. Jansen, E. M. M. de Brabander–van den Berg, E. W. Meijer, *Science* **1994**, *266*, 1226.
[12] D. K. Smith, F. Dietrich, *Chem. Eur. J.* **1998**, *4*, 1353.
[13] E. Donath, G. B. Sukhornkov, F. Caruso, S. A. Davis, H. Möhwald, *Angew. Chem. Int. Ed*. **1998**, *37*, 2202.
[14] F. Caruso, H. Lichtenfeld, M. Giersig, H. Möhwald, *J. Am. Chem. Soc.* **1998**, *120*, 8523.
[15] F. Caruso, R. A. Caruso, H. Möhwald, *Science* **1998**, *282*, 1111.
[16] H. Huang, E. E. Remsen, T. Kowalewski, K. L. Wooley, *J. Am. Chem. Soc.* **1999**, *121*, 3805.
[17] F. Baumann, M. Schmidt, B. Deubzer, M. Geck, J. Dauth, *Macromolecules* **1994**, *27*, 6102.
[18] F. Baumann, B. Deubzer, M. Geck, J. Dauth, S. S. Sheiko, M. Schmidt, *Adv. Mater*. **1997**, *9*, 955.
[19] F. Baumann, B. Deubzer, M. Geck, J. Dauth, M. Schmidt, *Macromolecules* **1997**, *30*, 7568.
[20] A. Becker, W. Köhler, B. Müller, *Ber. Bunsenges. Phys. Chem.* **1995**, *99*, 600.
[21] G. R. Strobl. *J. Appl. Cryst*. **1973**, *6*, 365.

Linear and Unanticipated Second-Order Nonlinear Optical Properties of Benzylic Amide [2]Catenane Thin Films: Evidence of Partial Rotation of the Interlocked Molecular Rings in the Solid State**

By *Torsten Gase, Daniela Grando, Pierre-Alain Chollet, François Kajzar,* Aden Murphy,* and *David A. Leigh**

In the past two decades there has been a widespread interest in developing organic materials for linear and nonlinear optical applications.[1] Catenanes,[2] molecules composed of mechanically interlocked rings, constitute an example of the diversity of compounds of unusual molecular architecture that are now within the reach of synthetic chemistry. Recently, catenanes have been proposed as possible elements in the development of components for nanoscale devices such as molecular switches, shuttles, and information storage systems.[3] The principle of operation of such devices is expected to be the control of the interlocked ring rotation through external stimuli (e.g., electri-

[*] Prof. F. Kajzar, Dr. T. Gase, Dr. D. Grando, Dr. P.-A. Chollet
LETI (CEA—Technologies Avancées), DEIN/SPE/GCO
CE Saclay
F-91191 Gif-sur-Yvette Cedex (France)

Dr. A. Murphy, Prof. D. A. Leigh
Centre for Supramolecular and Macromolecular Chemistry
Department of Chemistry, University of Warwick
Coventry CV4 7AL (UK)